# MMO: MEA

## CALIBRATION REPORT

| **Document under Configuration Control** | X |
|---|---|

| **Prepared by** | **Date** | **Signature:** |
|---|---|---|
| Andrey Fedorov | | |
| **Verified by** | | **Signature:** |
| Claude Austin | | |
| **Approved and Application authorized by:** | | **Signature:** |
| Jean Andre Sauvaud | | |

**Summary** : MEA FM calibration report and description of the calibration data record

**Keywords** : Calibration

**Annex:** Calibration Data

## I DISTRIBUTION LIST

| PROJECT | EXTERNAL DISTRIBUTION |
|---|---|
| C. AOUSTIN<br>E. LE COMTE<br>J.-A. SAUVAUD<br>J. ROUZAUD<br>P. ROUGER<br>Q.-M. LEE<br>H.-C. SERAN<br>M. PETIOT<br>C. GARAT<br>D. MOIRIN | Y. SAITO |

## II LIST OF ABBREVIATIONS

| | | | |
|---|---|---|---|
| **MMO** | Mercury Magnetosphere Orbiter | | |
| **MEA** | Mercury Electron Analyzer | | |
| **TBC** | To Be Completed | | |
| **TBD** | To Be Defined | | |
| **TBW** | To Be Worked | | |
| | | | |
| | | | |
| | | | |
| | | | |
| | | | |

## III DOCUMENT CHANGE RECORD

| Edition | Revision | Date | Modified pages | Reason for change / Observations |
|---|---|---|---|---|
| 0 | 0 | 04/12/2012 | | First drafty version |
| 1 | 0 | 25/01/2013 | all | Preliminary version |
| 2 | 0 | 15/03/2013 | all | Complete version |

**TABLE OF CONTENTS**

# 1. Scope of this document

This document contains a complete description of the MEA calibration setup, MEA calibration procedure and MEA calibration data. The document shows also the theoretical properties of the conceptual design to make a comparison the conception properties and the real instrument properties. To understand this document, reader should refer to the "MEA Instrument Design Report". The Annexes contains the tables of the supplementary data files and the electron beam calibration details.

# 2. Definitions

$E$ Incident electron energy, eV
$\Theta$ Elevation angle (see Figure 1,2)
$\Phi$ Azimuth angle (see Figure 1,2)
$U_{AN}$ Analyzer voltage
$U_{TOP}$ Top part of analyzer voltage
$K$ $E = U_{AN} \cdot K$
$K0$ The best $K$ for the current $\Theta$ and $\Theta$
$\Delta E/E$ Energy resolution of the analyzer
$P_{BEAM}$ electron beam flux $cm^{-2}\ s^{-1}$ as a function of the elevation angle
$\Omega_i$ one azimuthal sector aperture, $cm^2$ for fixed $\Theta$, $\Phi$, $U_{AN}$ , and $U_{TOP}$
$C_i$ count rate, $s^{-1}$ of one azimuthal sector
$G_i$ one sector geometrical factor, $cm^2\ sr\ eV/eV$
$G$ the total geometrical factor of the instrument, $cm^2\ sr\ eV/eV$ (used for numerical simulation)
$HV_{MCP}$ The MCP high voltage, V, measured at the HV unit level.

Figures 1,2,3 show the MEA axis definition, spherical frame of measurement definitions, azimuthal sectors (anodes) numbering and theirs position in the MEA frame and in the MMO frame. Note that Figure 2 gives looking directions of the anodes.

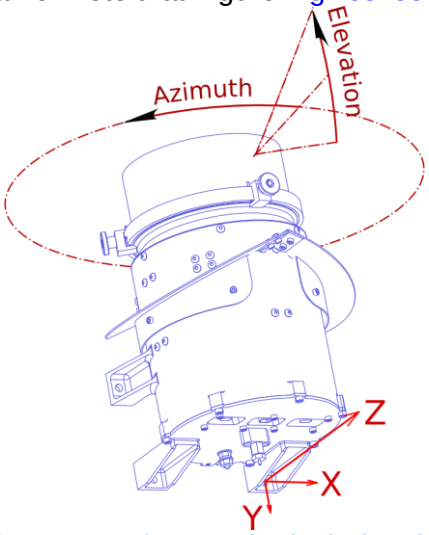


Figure 1 MEA frame and spherical angles

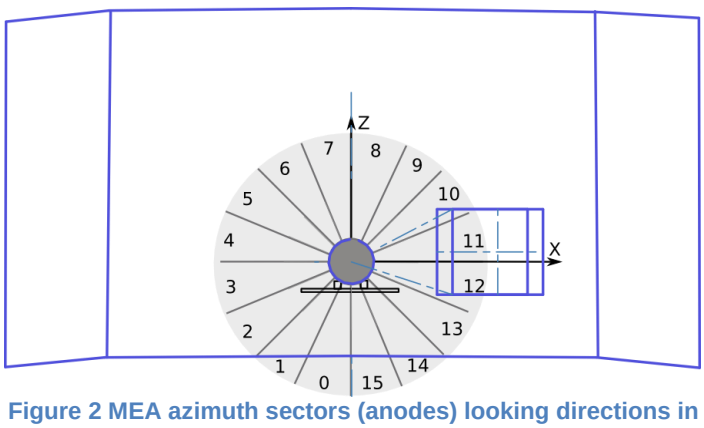


Figure 2 MEA azimuth sectors (anodes) looking directions in the MMO frame

## 3. MEA theoretical properties

MEA theoretical properties were obtained with a realistic 3-D numerical model.
The results of ray tracing are shown in Figures 3,4. The summary of the numerical results is in Table 1 in the bottom of this section. Technically, the instrument response was obtained as follows:

1. Set constant $U_{AN}$ , $U_{TOP}$
2. Illuminate the sensor by the parallel uniform electron beam with variable:
   (a) Energy
   (b) Elevation angle
   (c) Azimuth angle
3. Calculate $\Omega_i$ of the sensor for each value of the energy, azimuth, and elevation
4. Do the same for several $U_{TOP}$ $/U_{AN}$ values, that should represent the set of geometrical factors of the instrument.

Figure 3 represents the variation of the instrument responses with geometrical factor (note that elevation angle definition here is opposite to the Calibration Elevation angle, Figures 1 and 13). Figure 4 shows the profile of $G$ as a function of $U_{TOP}$ $/U_{AN}$.

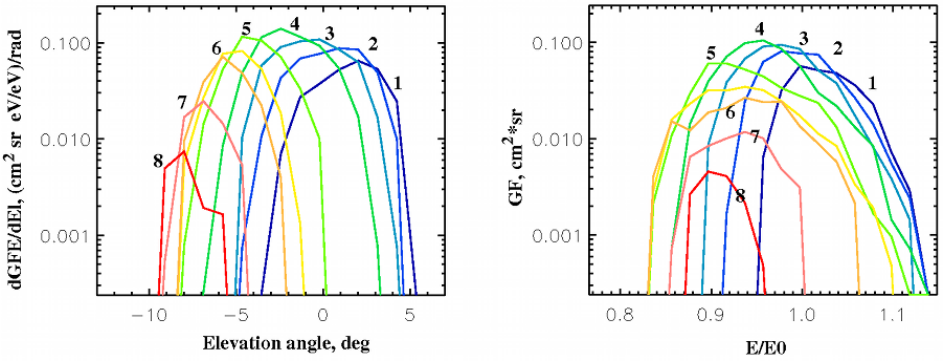


Figure 3 Elevation (left) end energy responses of MEA for different geometrical factors

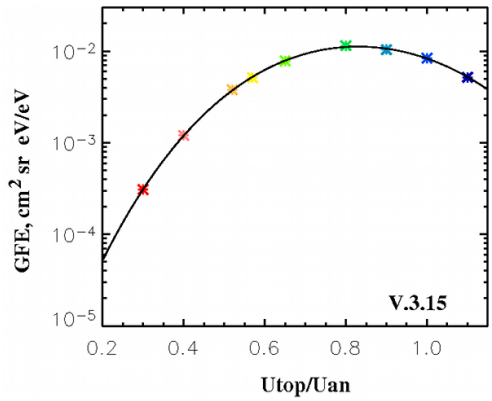


Figure 4 G as a function of Utop/Uan

The corresponding best fit formula is:

$$G[cm^2\ sr\ eV/eV] = -15.05 + 32.65 \cdot \left(\frac{U_{Top}}{U_{An}}\right) - 36.18 \cdot \left(\frac{U_{Top}}{U_{An}}\right)^2 + 19.14 \cdot \left(\frac{U_{Top}}{U_{An}}\right)^3 - 5.31 \cdot \left(\frac{U_{Top}}{U_{An}}\right)^4$$

| # | $U_{TOP}$ $/U_{AN}$ | $K$ | $\Delta E/E$ | $G, cm^2\ sr\ eV/eV$ |
|---|---|---|---|---|
| 1 | 1.1 | 10.2 | 0.09 | $0.51 \cdot 10^{-2}$ |
| 2 | 1.0 | 9.95 | 0.10 | $0.83 \cdot 10^{-2}$ |

| | | | | |
|---|---|---|---|---|
| 3 | 0.9 | 9.75 | 0.11 | $1.03 \cdot 10^{-2}$ |
| 4 | 0.8 | 9.56 | 0.11 | $1.15 \cdot 10^{-2}$ |
| 5 | 0.65 | 9.37 | 0.13 | $0.78 \cdot 10^{-2}$ |
| 6 | 0.57 | 9.34 | 0.15 | $0.51 \cdot 10^{-2}$ |
| 7 | 0.52 | 9.34 | 0.14 | $0.37 \cdot 10^{-2}$ |
| 8 | 0.4 | 9.25 | 0.10 | $0.12 \cdot 10^{-2}$ |
| 9 | 0.3 | 9.03 | 0.07 | $0.03 \cdot 10^{-2}$ |

Table 1 Summary of MEA numerical simulation

# 4. Calibration setup

## 4.1 Mechanical setups

The IRAP big vacuum chamber was used for MEA calibration. There are three type of tests and correspondingly three types of mechanical setups:

- Full calibration setup
- MCP characterization setup
- UV contamination test setup

### 4.1.1 Full calibration setup

The mechanical MEA setup is shown in Figure 5. The center of the beam is matched to the line of sight of the instrument. The Θ rotation center is very close to its line of sight. The corresponding photo is shown in Figure 6. This figure shows as well the beam monitor and the magnetometer dedicated to the run time reading of the magnetic filed in the vicinity of the instrument.

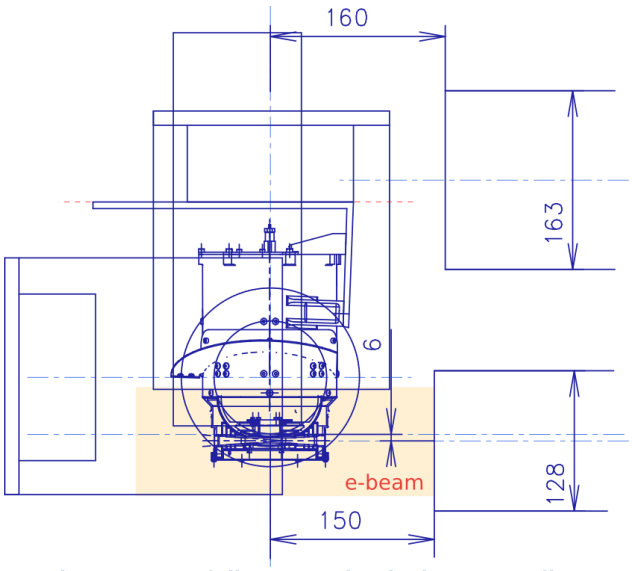


Figure 5 MEA full test mechanical setup. Yellow rectangular shows the electron beam size

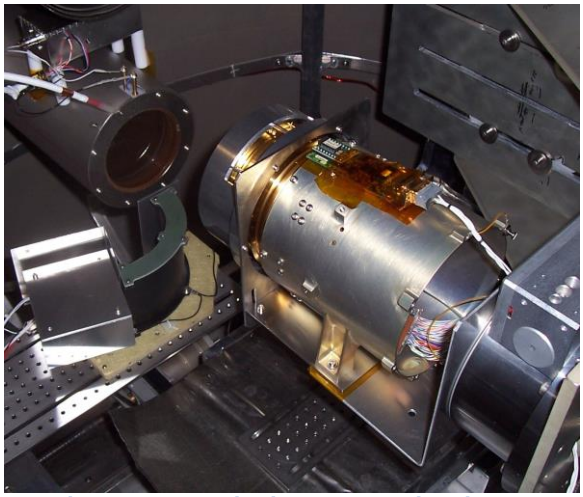

**Figure 6 MEA-1 in the vacuum chamber. A magnetometer is glued to the sensor housing. The instrument is turned on 90° in elevation. Note the thermal shield simulator above the instrument aperture.**

To make the calibration results relevant, the calibration has been made with a realistic simulator of the instrument thermal shield. The Earth's magnetic field inside the vacuum chamber is compensated by the Helmholtz coils. Continuous measurements of the residual magnetic field and its run-time automatic adjustment allows to keep the maximal value of the magnetic field about $0.5\mu T$. See the beam properties in Section 4.2 and Annex 1.

### 4.1.2 MCP characterization setup

MCP characterization setup is quite different for the full calibration one:

a. The sensor is disassembled to expose MCP directly to the beam (see Figure 7);
b. The special attractive diaphragm is installed around the MCP ring to avoid contamination of the measurements by secondary electrons (not shown). The diaphragm potential is +5V.
c. The MCP is testes by a needle-like electron beam generated by a special Y-Z mobile electron gun (Figure 7)

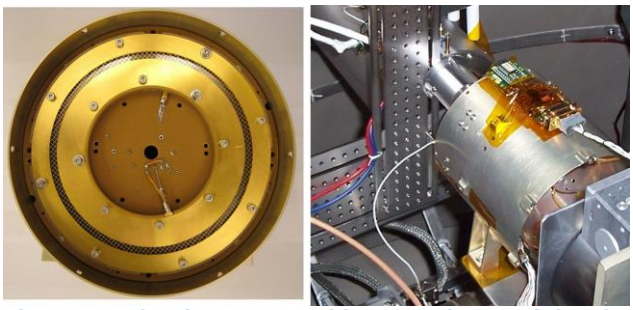

**Figure 7 Left: The sensor with no analyzer, Right: the MCP characterization setup. One can see the needle-like beam electron gun.**

### 4.1.3 UV contamination test setup

UV contamination test has been made with HAMAMATSU Deuterium lamp L7292. The setup is shown in Figure 8. The beam photon rate in the VUV range (~160nm) at the instrument level is $2.4 \cdot 10^{11}\ s^{-1}\ cm^{-2}$.

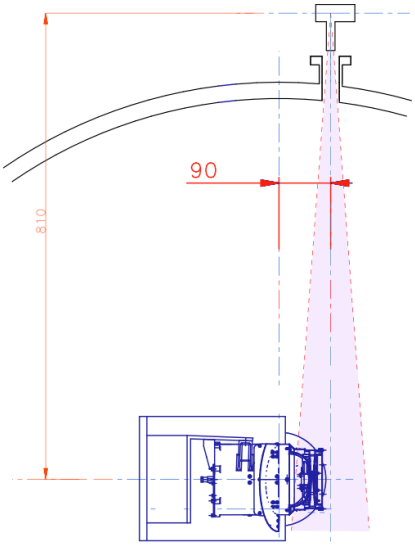


Figure 8 UV test setup

## 4.2 Beam properties

For each calibration stage the electron beam absolute measurements are performed. The characteristic beam properties are shown in Figure 9. To increase the beam intensity, the UV lamp was located close to the photocathode. This leads to a non-uniformity of the beam as it is shown in Figure 9. Such a distribution is measured by scanning the beam by a dedicated monitor unit with a pin-hole entrance (Figure 6). At the same time we measure the total electron current leaving the photochathode. The monitor count rate is converted to the real flux assuming that the total count of a 2D distribution corresponds to the total electron current of the photocathode. The beam flow $P_{BEAM}$ for each elevation position of the sensor was recalculated as it is shown in Figure 9 bottom. This distribution is calculated by averaging of the original 2D distribution inside a rectangle $12 \times 5mm$. The position of this rectangle in the 2D beam flux distribution is calculated from the mechanical setup shown in Figure 5. The beam distribution was measured for each calibration run. The beam measurements corresponding to each calibration run are shown in Annex 2.

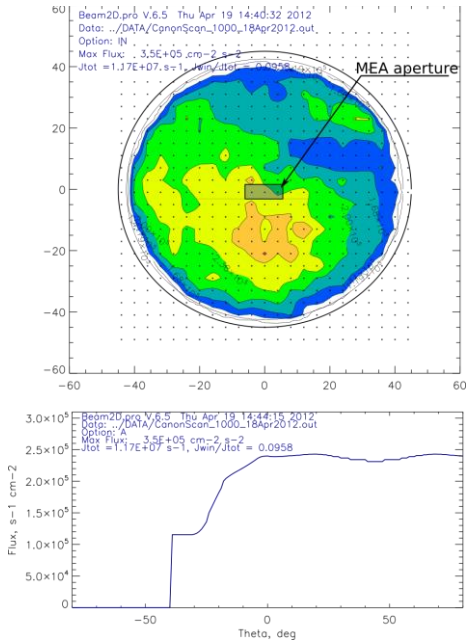


Figure 9 Electron beam properties

# 5. Calibration results and data record

## 5.1 MCP characterization

### 5.1.1 MCP image

MCP image have been measured to provide information about MCP heals and MCP efficiency uniformity. To do this the MCP has been scanned by a needle-like electron beam. The results of such scan for MEA-1 and MEA-2 are shown in Figure 10. The distributions show that all anodes (except MEA-1 closed anodes are functional, and there is not significant efficiency difference.

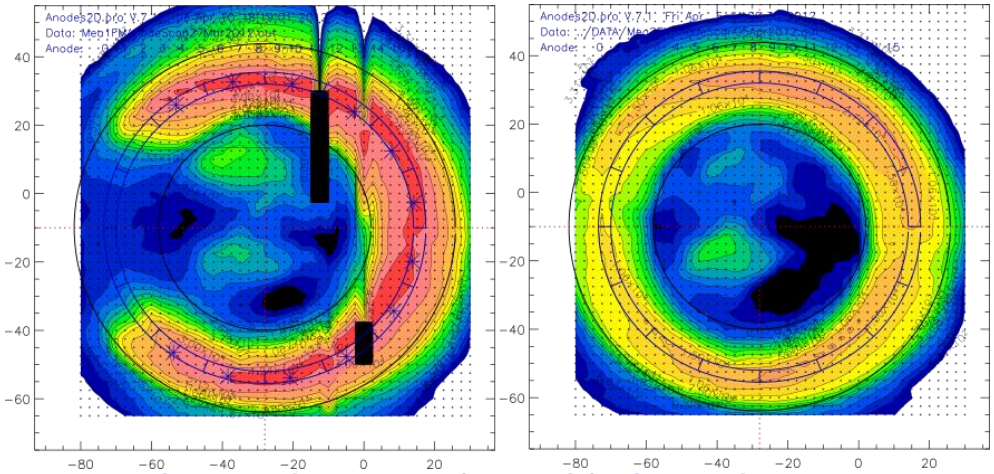

Figure 10 Left: MEA-1 MCP image, Right: the same for MEA-2

### 5.1.2 MCP count profile

MCP anodes counts as a function of $HV_{MCP}$ are shown in Figure 11. The measurements was done with a needle-like beam positioned in the anodes gravity centres (points marked by stars in Figure 10, left). Note that $HV_{MCP}$ gives the voltage at the HV unit output. The real MCP bias is 400V less. The working point of both MCPs (MEA-1 and MEA-2) is chosen as 2750V. The corresponding text data of the calibration package see in Annex 2.

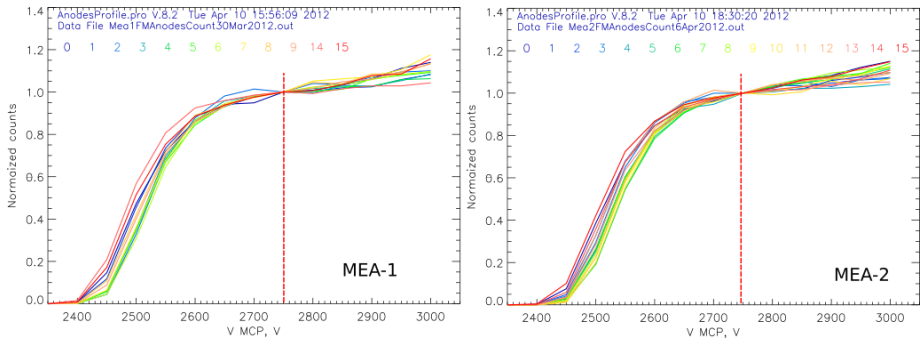


Figure 11 MCP normalized count as a function of the $HV_{MCP}$

### 5.1.3 MCP noise

MCP noise has been measured for MEA-1 only since there are completely obscured anodes. The results are shown in Figure 12. See the corresponding text file in Annex 1.

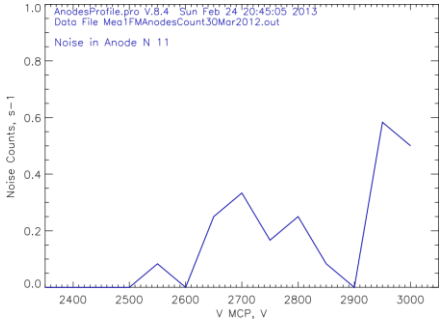


Figure 12 One anode MCP noise versus $HV_{MCP}$

### 5.1.4 MCP efficiency variations

MCP anode-by-anode efficiency variation was made at the same time as the count v. $HV_{MCP}$. The measurement conditions are as follows:

- Electron beam: 1000eV
- $HV_{MCP} = 2750\ V$

The results are shown in Figure 13. Corresponding best fit formulas are as follows:

$$Rel.Count = 0.10 \cdot \sin((N_{Anode} - 4.02) \cdot 4\pi/16 \quad \text{MEA-1}$$
$$Rel.Count = 0.22 \cdot \sin((N_{Anode} - 4.64) \cdot 4\pi/16 \quad \text{MEA-2}$$

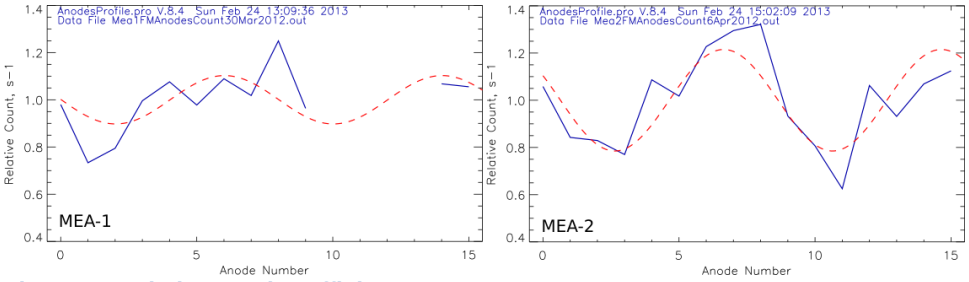


Figure 13 Relative anodes efficiency

The corresponding text files are described in Annex 1.

### 5.1.5 MCP dead time

The MCP dead time of one anode was measured by defocused beam with a known ratio between the intensity in the beam center and beam periphery. Thus, varying, the beam flux, we have a linear count at one anode and saturated count in another anode. The results are shown in Figure 14. The one anode saturation level is the same for the both sensors. The MCP-amplifier chain saturation can be describes by formula:

$$C_i = CO_i/(1 + CO_i \cdot \tau)$$

Here $CO_i$ is an incident electron rate of one anode and $\tau$ is defined from the table:

| | MEA-1 | MEA-2 |
|---|---|---|
| $\tau, \mu s$ | 1.2 | 1.22 |

The corresponding data file see in Annex 1.

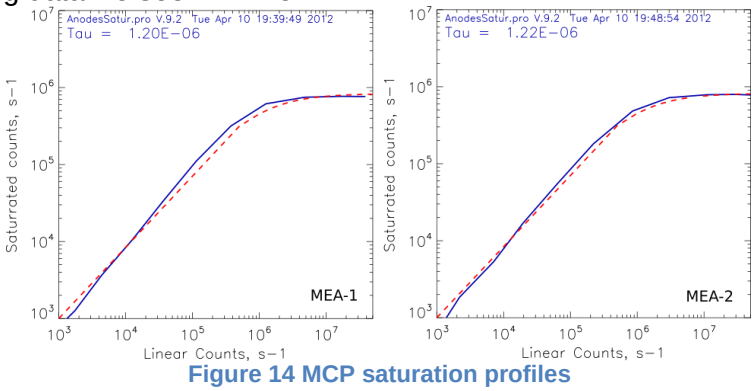


Figure 14 MCP saturation profiles

## 5.2 MEA full calibration

### 5.2.1 Full calibration procedure

The full MEA-1 and MEA-2 calibration was made in the coordinate frame shown in Figure 15. The beam properties is as follows:

| Item | Value | Comment |
|---|---|---|
| Beam Energy | 1000 eV | To avoid any influence of the residual magnetic field |
| Beam number flux density MEA 1 | about $1.7 \cdot 10^5\ cm^{-2}\ s^{-1}$ | See Annex 2 |
| Beam number flux density MEA 2 | about $2.4 \cdot 10^5\ cm^{-2}\ s^{-1}$ | See Annex 2 |

Table 2 Full calibration run conditions

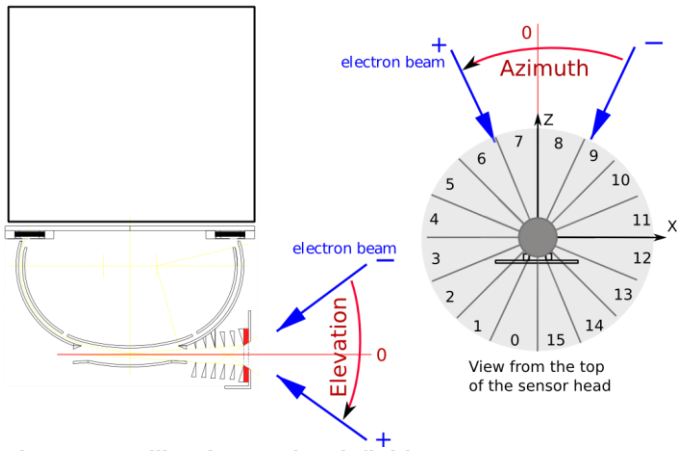


Figure 15 Calibration angles definition

A brief description of the calibration scheme:

| Dimension | Range | Step | N steps |
|---|---|---|---|
| Azimuth, $\Phi$ | $-166° \div +166°$ | $2°$ | 167 |
| Elevation, $\Theta$ | $-8° \div +18°$ | $1.5°$ | 18 |
| Analyzer voltage, $\Delta K/K_0$ | $0.78 \div 1.24$ | 0.025 | 15 |
| Top part voltage MEA-1, $U_{TOP}\ /U_{AN}$ | {1.0, 0.8, 0.52, 0.37, 0.28} | | 5 |
| Top part voltage MEA-2, $U_{TOP}\ /U_{AN}$ | {1.0, 0.8, 0.42, 0.34, 0.27} | | 5 |

Table 3 The full calibration scheme

For each Azimuth angle $\Phi$, we make a scan over elevation angle $\Theta$. For each angular position we test the set of geometrical factors values. For each value of geometrical factor attenuation we scan the analyzer voltage.

### 5.2.2 Full calibration results

The main raw result of the full calibration could be expressed as an anode effective aperture ($\Omega_i$) as a function of azimuthal angle $\Phi$, elevation angle $\Theta$, and energy ($U_{AN}$ actually) for all geometrical factor attenuation levels. The raw data converted from counts to $\Omega_i$ are presented in a self-described text file. See Annex 1 for details. The integral of these data over the energy and $\Theta$ are shown in Figure 16. One can see the modulation of the geometrical factor as a function of beam azimuth increasing when geometrical factor is reducing. The modulation of K factor as a function of the anode number (azimuth) is shown in Figure 17. The variation of the central angle $\Theta$ as a function of the anode number (azimuth) and the G level is shown in Figure 18. Figures 19 and 20 show the energy and elevation responses for different anodes and different G levels. The dashed curves in these plots shows the polynomial fit that allows to define the $\Delta E/E$ and $\Delta\Theta$ with high accuracy. Anodes geometrical factor versus the $U_{TOP}/U_{an}$ value is shown in Figure 21. The theoretical profile obtained from the numerical simulation is shown by dashed curve. The attenuation factor values, that include the grid transparences and MCP efficiency are as follows:

| | MEA-1 | MEA-2 |
|---|---|---|
| Theory/calibration factor | 20 x 4.0 | 5.5 |

The corresponding final values, as $G_i$, $K$, $\Theta_0$, $\Delta E/E$, $\Delta\Theta$, etc, applicable for the data analysis are given in the dedicated text files. See Annex 1 for details.

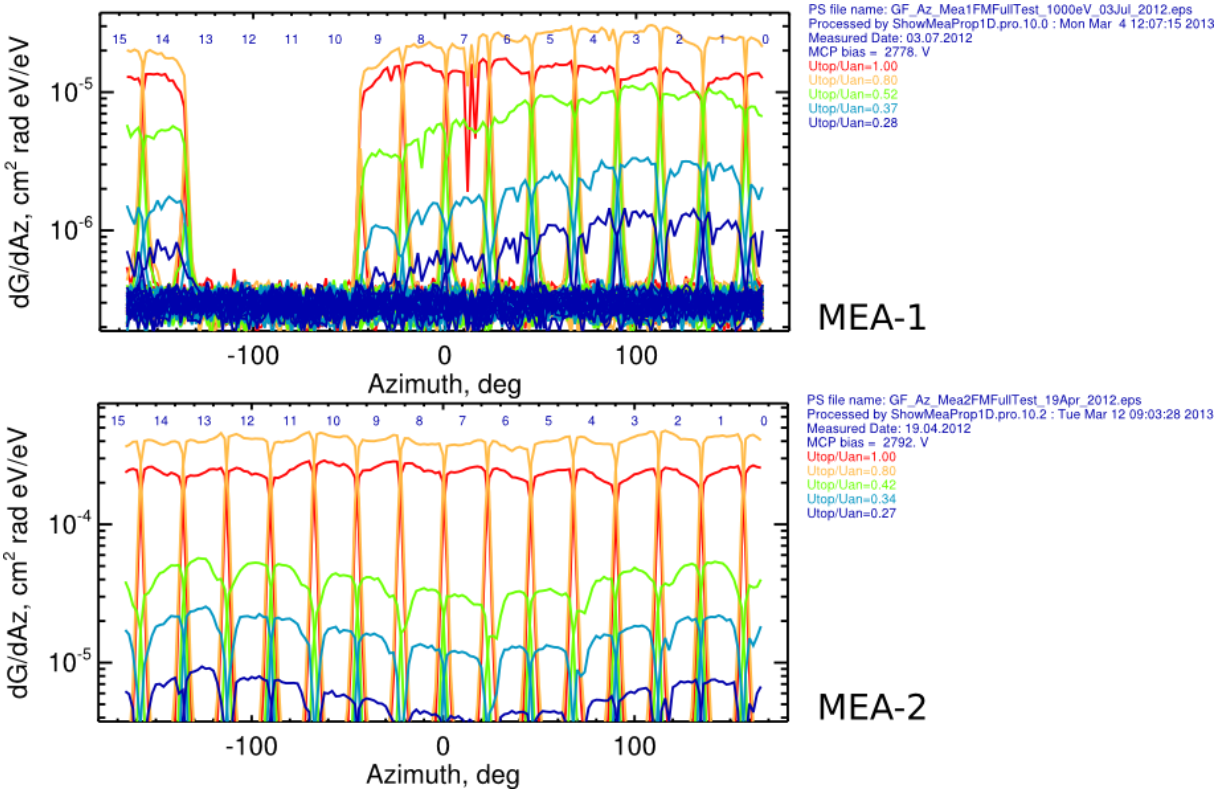


**Figure 16 Azumuthal density of one anode geometrical factor**

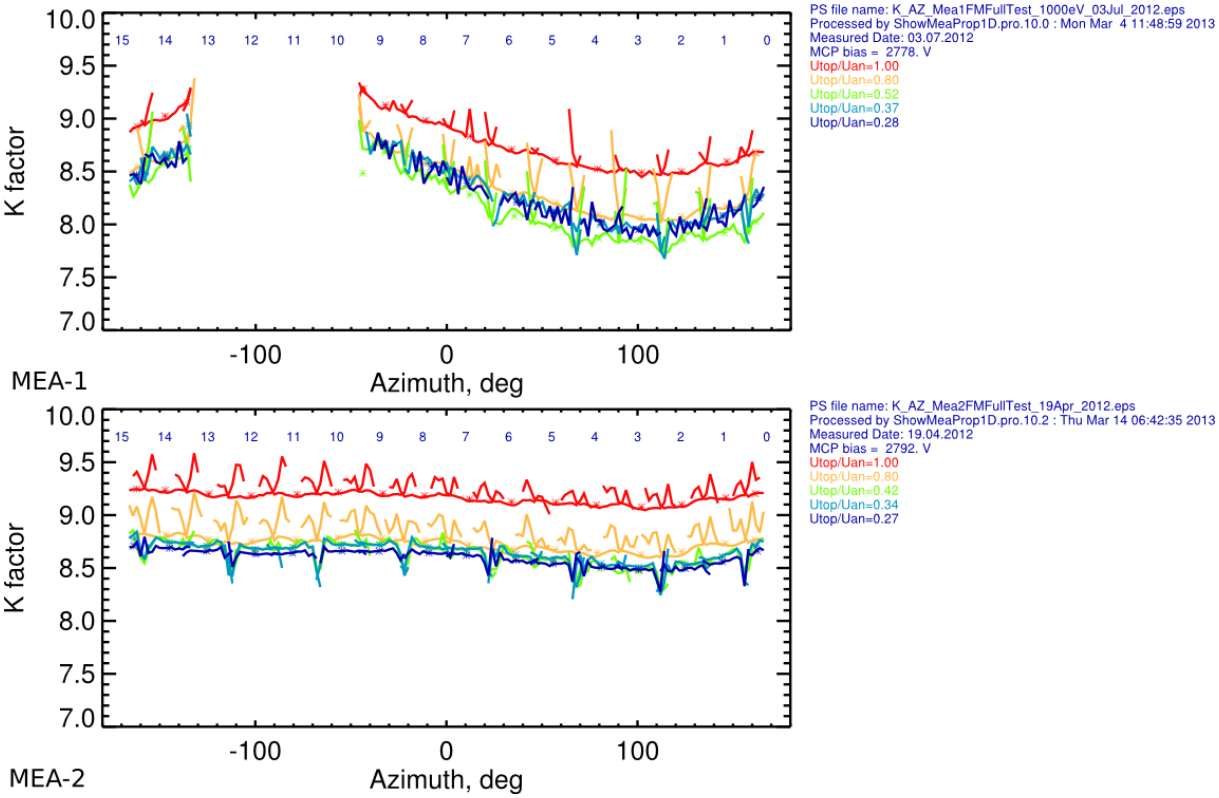


**Figure 17 Factor K variation along G levels as a function of azimuth and anode number**

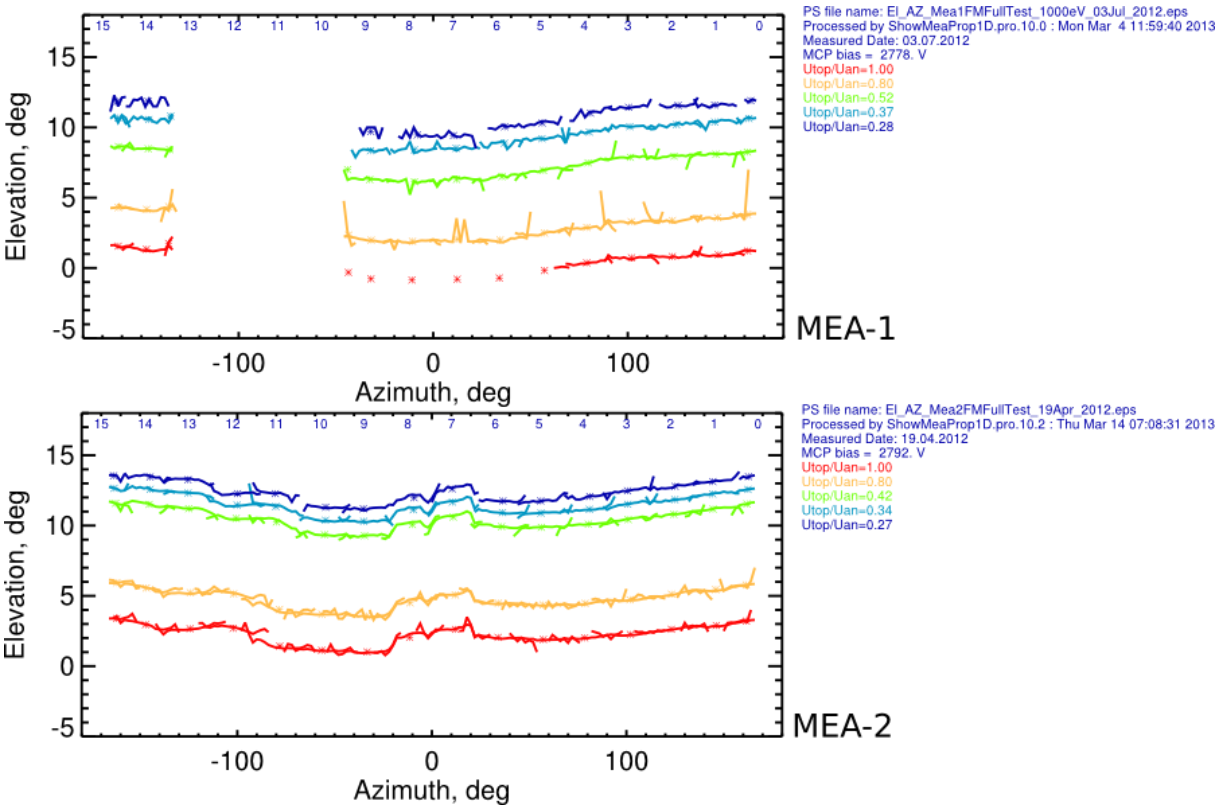


**Figure 18 Central elevation angle as a function of the G level and athimuth**

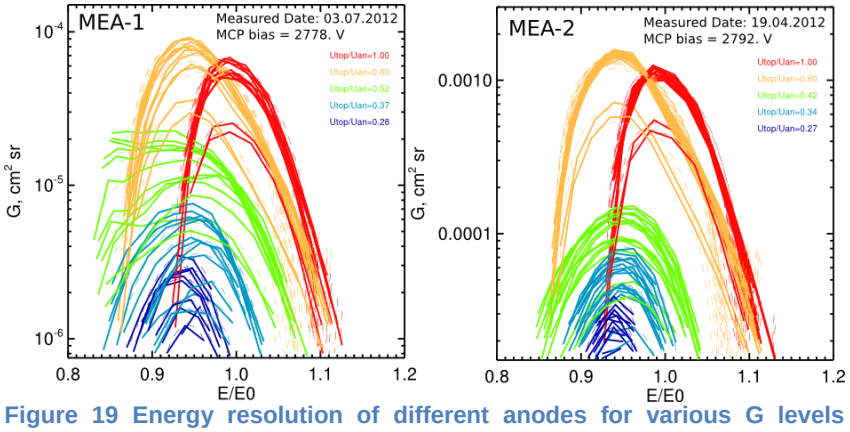


**Figure 19 Energy resolution of different anodes for various G levels (color)**

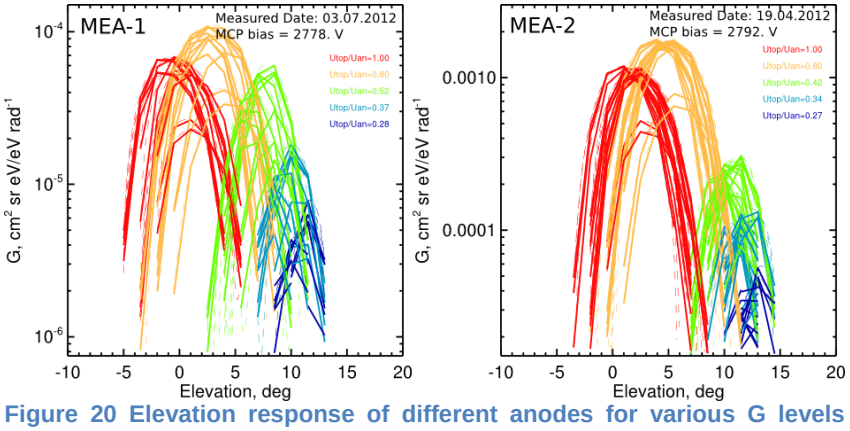


**Figure 20 Elevation response of different anodes for various G levels (color)**

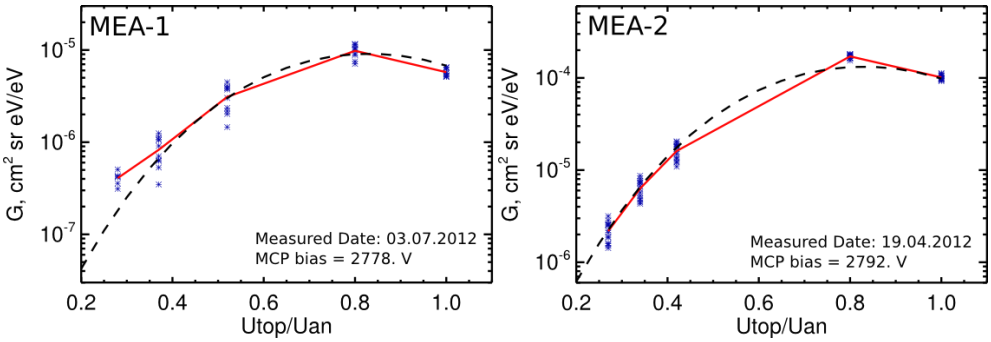


**Figure 21 Anodes geometrical factors as a functions of $U_{TOP}/U_{an}$. The dashed lines show the theoretical profile scaled with appropriate factor (see the text).**

## 5.3 UV contamination results

UV contamination test results are shown in Figure 22. The strong count at the small energies show the photoelectrons emitted inside the instrument an in the vacuum chamber. One can see that the maximal background is less than 1 per second per anode.

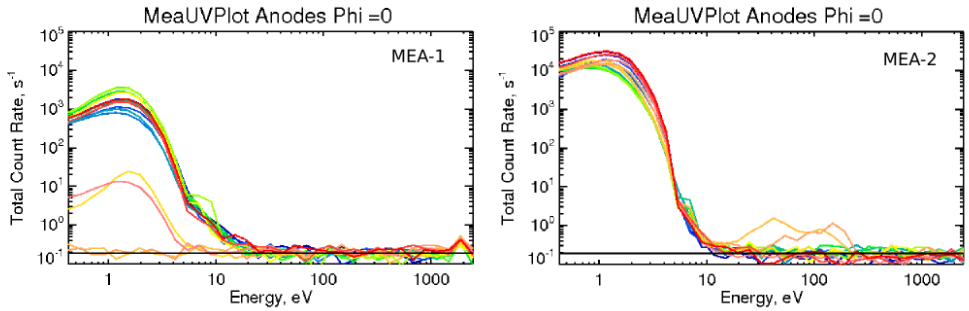


Figure 22 UV contamination tests results

## 6. Summary of the calibration results

The anodes average of the calibration results are shown in Tables 4 and 5. These data are not applicable for the data processing and should be used for reference purposes.

| $U_{TOP}/U_{Analyz}$ | 1.0 | 0.8 | 0.42 | 0.34 | 0.27 |
|---|---|---|---|---|---|
| GF $cm^2$ sr eV/eV | $1.01 \cdot 10^{-4}$ | $1.71 \cdot 10^{-4}$ | $1.61 \cdot 10^{-5}$ | $6.32 \cdot 10^{-6}$ | $2.17 \cdot 10^{-6}$ |
| $GF_0/GF$ | | 1.0 (1) | 10.65 (6) | 27.09 (20) | 78.80 (60) |
| Θ deg | 2.3 | 4.8 | 10.5 | 11.6 | 12.5 |
| ΔΘ deg | 5.35 | 5.77 | 3.45 | 2.98 | 2.73 |
| K | 9.17 | 8.73 | 8.64 | 8.65 | 8.61 |
| Δ E/E | 0.095 | 0.119 | 0.121 | 0.087 | 0.044 |

Table 4 MEA-2 calibration summary

| $U_{TOP}/U_{Analyz}$ | 1.0 | 0.8 | 0.52 | 0.37 | 0.28 |
|---|---|---|---|---|---|
| GF $cm^2$ sr eV/eV | $5.75 \cdot 10^{-6}$ | $9.80 \cdot 10^{-6}$ | $3.10 \cdot 10^{-6}$ | $8.27 \cdot 10^{-7}$ | $3.29 \cdot 10^{-7}$ |
| $GF_0/GF$ | | 17.46 (20) | 55.21 (60) | 207 (250) | 520 (1000!) |
| Θ deg | 0.3 | 3.0 | 7.4 | 9.6 | 10.8 |
| ΔΘ deg | 5.39 | 5.89 | 3.86 | 3.32 | 2.73 |
| K | 8.75 | 8.35 | 8.16 | 8.30 | 8.29 |
| Δ E/E | 0.123 | 0.155 | 0.158 | 0.115 | 0.074 |

Table 5 MAE-1 Calibration summary

# ANNEX 1 SUPPLEMENTARY DATA FILES

The calibration data package is in the file MEA_FM_Calibration_Data_2_0_15_Mar_2013.zip attached to this document. The calibration data package consists of the following files:

| What is it? | MEA-1 file | MEA-2 file |
|---|---|---|
| MCP count as a function of $HV_{MCP}$ | MEA1_FM_MCP_Count_Voltage.txt | MEA2_FM_MCP_Count_Voltage.txt |
| MCP one anode background count rate as a function of $HV_{MCP}$ | MEA1_FM_MCP_Noise.txt | No data |
| MCP relative efficiency | MEA2_FM_MCP_Rel_Eff.txt | MEA2_FM_MCP_Rel_Eff.txt |
| MCP saturation profile | MEA1_FM_MCP_Satur.txt | MEA2_FM_MCP_Satur.txt |
| Full calibration original data | Mea1FMFullTest_1000eV_03Jul_2012.txt | Mea2FMFullTest_1000eV_19Apr_2012.txt |
| Full calibration applicable data | Mea1_FM_Properties_1000eV_03Jul_2012.txt | Mea2_FM_Properties_1000eV_19Apr_2012.txt |

# ANNEX 2 ELECTRON BEAM CALIBRATION

The beam profile as a function of MEA $\theta$ taken on 18 Apr 2012 for the MEA-2 full calibrations is:

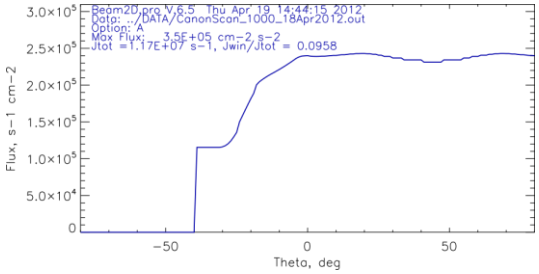


**Figure 23 Beam profile on 18 Apr 2012**

The beam profile as a function of MEA $\theta$ taken on 11 Jun 2012 for the MEA-1 full calibrations is:

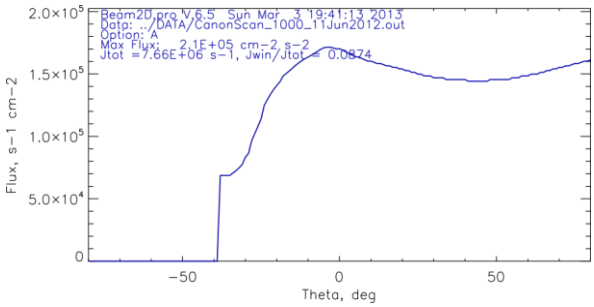


**Figure 24 Beam profile on 11 Jun 2012**